CSIRO PUBLISHING

Australian Journal of Physics

Volume 53, 2000
© CSIRO Australia 2000

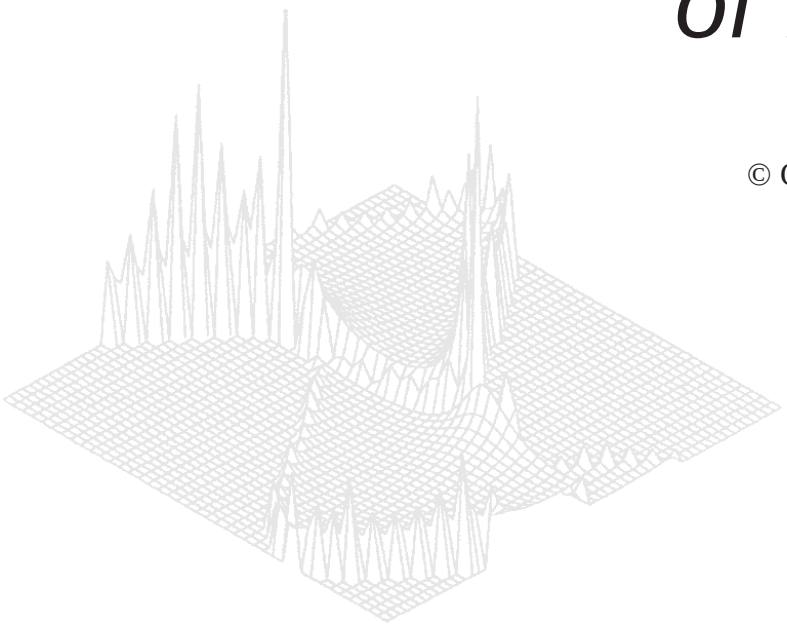

A journal for the publication of
original research in all branches of physics

www.publish.csiro.au/journals/ajp

All enquiries and manuscripts should be directed to
Australian Journal of Physics
CSIRO PUBLISHING
PO Box 1139 (150 Oxford St)
Collingwood Telephone: 61 3 9662 7626
Vic. 3066 Facsimile: 61 3 9662 7611
Australia Email: peter.robertson@publish.csiro.au

Published by **CSIRO** PUBLISHING
for CSIRO Australia and
the Australian Academy of Science

Aust. J. Phys., 2000, **53**, 35–51

Coherent and Phonon-assisted Tunnelling in Asymmetric Double Barrier Resonant Tunnelling Structures*

Jun-jie Shi,[A,B,C] *B. C. Sanders*[A] *and Shao-hua Pan*[A,B,D]

[A] Department of Physics, Macquarie University,
North Ryde, NSW 2109, Australia.
[B] China Center of Advanced Science and Technology (World Laboratory),
PO Box 8730, Beijing 100080, P.R. China.
[C] On leave from Department of Physics, Henan Normal University,
Xinxiang 453002, Henan, P.R. China.
[D] Institute of Physics, Chinese Academy of Sciences,
PO Box 603, Beijing 100080, P.R. China.

Abstract

We present a theory for calculating the phonon-assisted tunnelling current in asymmetric double barrier resonant tunnelling structures (DBRTS), in which all of the phonon modes including the interface modes and the confined bulk-like LO phonons and the conduction band nonparabolicity are considered. An important physical picture about coherent and phonon-assisted tunnelling is given. The coherent tunnelling current can be directly determined by both the width of the resonant level and the peak value of the transmission coefficient at the resonant level. The phonon-assisted tunnelling current mainly comes from electron interaction with higher frequency interface phonons (especially the interface phonons localised at either interface of the left barrier). Phonon-assisted tunnelling makes a significant contribution to the valley current. The subband nonparabolicity strongly influences on electron–phonon scattering and current-to-voltage characteristics. A specially designed asymmetric DBRTS may have an improved performance over the symmetric DBRTS.

1. Introduction

There has been significant interest recently in polar semiconductor resonant tunnelling diodes (RTD) for their special device applications, as well as for their unique physical properties (Mizuta and Tanoue 1995; Sun *et al.* 1998). One of the most important RTD are the so-called double barrier resonant tunnelling structures (DBRTS) which consist of an undoped quantum well (QW) layer sandwiched between undoped barrier layers and heavily doped contact layers which offer tunnelling electrons as an emitter and collector. A DBRTS is an open quantum system in which the electronic states are scattering states with a continuous distribution in energy space, rather than bound states with a discrete energy spectrum. The quasi-bound states (resonant states) are formed in the QW which accommodate electrons for a certain dwell time. There are many interesting physical problems associated with resonant tunnelling. Hence, the DBRTS has attracted great interest and has been investigated both from the

* Refereed paper based on a talk presented to the Workshop on Nanostructures and Quantum Confinements, held at the Australian National University, Canberra, in December 1998.

© CSIRO 2000 10.1071/PH99037 0004-9506/00/010035$10.00

standpoint of quantum transport physics and also its application in functional quantum devices since the pioneering work of Tsu and Esaki (1973) and Chang *et al.* (1974).

The most important practical feature of the DBRTS for electronics is its negative differential resistance (NDR), which is particularly useful for high-frequency resonant tunnelling and rapid switching devices. For a given DBRTS, a current peak exists in its current-to-voltage characteristic curve for a certain bias voltage V_r. If a bias voltage $V > V_r$, the slope of this curve becomes negative, and an obvious NDR can be observed. The NDR can be quantified by the peak-to-valley ratio (PVR) of the current-to-voltage characteristic curve. A large PVR and a low valley current are desirable for most RTD device applications. Thus, understanding the mechanism of the valley current is quite important for designing better RTDs.

Generally speaking, phonon-assisted tunnelling, $\Gamma - X$ intervalley tunnelling, impurity scattering, the interface roughness scattering and the tunnelling of quasi-two-dimensional subband electrons in a pseudo-triangular well in the emitter can cause the valley current (Mizuta and Tanoue 1995; Roblin and Liou 1993; Sun *et al.* 1998). For a polar semiconductor DBRTS, the effects of electron scattering on resonant tunnelling are very important and inevitable especially at room temperature. The electrons in the DBRTS may emit phonons during the resonant tunnelling process. Resonant tunnelling accompanied by a phonon emission is called *phonon-assisted tunnelling* (Mizuta and Tanoue 1995). In general, the probability of this process is relatively small compared with that of the main resonant tunnelling process. Phonon-assisted tunnelling in RTD has attracted much attention in the recent literature because of its importance in controlling the NDR.

Longitudinal-optical (LO) phonon-assisted resonant tunnelling at low temperature was first observed experimentally by Goldman *et al.* (1987) using an $Al_{0\cdot4}Ga_{0\cdot6}As$(85 Å)/GaAs(56 Å)/$Al_{0\cdot4}Ga_{0\cdot6}As$(85 Å) DBRTS. They found a small current peak in the valley region at $4\cdot2$ K with a magnitude of about $0\cdot04$ of the main peak. This peak was interpreted as being due to a single LO phonon-emission-assisted resonant tunnelling process. Subsequently, several studies have reported on phonon-assisted tunnelling in DBRTS at low temperatures. Leadbeater *et al*. (1989) investigated the current–voltage characteristics of DBRTS in the presence of a quantising magnetic field perpendicular to the barriers. Cai *et al.* (1989) studied one-dimensional electron tunnelling in an arbitrarily shaped barrier in the presence of electron–phonon scattering. Chevoir and Vinter (1989) calculated the LO phonon scattering contribution to electron tunnelling through an RTD. Wingreen *et al.* (1989) further investigated the resonant tunnelling transmission probability for an electron interacting with phonons and inelastics scattering in DBRTS. Turley and Teitsworth (1991*a*, 1991*b*, 1992, 1994) studied phonon-assisted tunnelling in symmetric DBRTS. Mori *et al.* (1992) investigated the effects of electron–interface–phonon interaction on resonant tunnelling in symmetric double barrier heterostructures. Mains and Haddad (1988) studied phonon-scattering-assisted tunnelling in RTD at room temperature by using the Wigner function method. Roblin and Liou (1993) derived an envelope equation by using the generalised Wannier function basis set and further investigated three-dimensional scattering-assisted tunnelling in RTD.

Asymmetric semiconductor heterostructures, such as asymmetric DBRTS and QW, have also attracted much attention due to their special device applications in recent years (Chen *et al.* 1991; Shi and Pan 1995, 1996; Schmidt *et al.* 1996; Orellana *et al.* 1996; Shi *et al.* 1997, 1998). It is believed that the phonon modes in polar semiconductor heterostructures are much more complicated than those of the bulk materials. The presence of interfaces in heterostructures necessarily alters the phonon modes and their interaction with electrons. Hence, the study of optical-phonon modes and their interaction with electrons in various heterostructures including asymmetric DBRTS and QW is imperative for analysing experiments and for device applications. Recently, optical-phonon modes, electron–phonon interaction and scattering, and polaron effects in asymmetric QW have been investigated in detail (Shi and Pan 1995, 1996; Shi *et al.* 1997). Some interesting results, such as the forbidden-frequency behaviour of the interface optical phonon modes and the anomalous phenomenon of the electron–phonon interaction in asymmetric QW caused by structural asymmetry has been found (Shi and Pan 1995, 1996). Moreover, Chen *et al.* (1991) pointed out that NDR can be tuned when asymmetric barriers are used in RTD. Asymmetric double barrier heterostructures may vary the amount of charge accumulation in the QW so that the current-to-voltage characteristics can be modified (Schmidt *et al.* 1996; Orellana *et al.* 1996). However, as we know, little theoretical work has been done on the electron–phonon interaction and scattering, or the phonon-assisted tunnelling in important asymmetric DBRTS at room temperature in the presence of the electron–phonon interaction, despite the great theoretical and practical importance of this work. It is thus worth while investigating the optical-phonon modes, the electron–phonon interaction and scattering and the phonon-assisted tunnelling in asymmetric DBRTS. The main purpose of this paper is to investigate the electron–phonon scattering and the phonon-assisted tunnelling in asymmetric DBRTS at room temperature and to show the advantages of asymmetric DBRTS for making the RTD. The phonon-assisted tunnelling physical picture is further clarified. We give the theory for the electron–phonon interaction and scattering and for the phonon-assisted tunnelling in asymmetric DBRTS in Section 2, present the numerical results and physical analysis in Section 3, and draw some conclusions in Section 4.

2. Theory

(2a) Electron–Phonon Interaction and Scattering in Asymmetric DBRTS

In order to calculate the phonon-assisted tunnelling current, let us first investigate the electron–phonon interaction and scattering in an asymmetric DBRTS. Within the framework of the dielectric continuum model, optical phonon modes and the electron–phonon interaction Fröhlich-like Hamiltonian $H_{\mathrm{e-ph}}$ can be conveniently obtained. The electron–phonon scattering rate W can be calculated according to the Fermi golden rule. For an asymmetric DBRTS we can obtain the scattering rate due to interface phonons as follows (Shi and Pan 1996):

$$W^{(i\to f)}(\vec{k}_i, E_z) = \frac{e^2}{16\pi\varepsilon_0}\sum_m \int d^2\vec{k}\frac{1}{\omega_m(k)\cdot k} \mid F_m(k) \mid^2 \delta(\varepsilon_i - \varepsilon_f \pm \hbar\omega_m(k)) \times (N_{\mathrm{ph}} + \tfrac{1}{2} \mp \tfrac{1}{2})\delta_{\vec{k}_i, \vec{k}_f \mp \vec{k}}\,, \tag{1}$$

and the rate due to confined LO phonons is

$$W^{(i\to f)}(\vec{k}_i, E_z) = \frac{e^2}{2\pi\varepsilon_0}\sum_{\nu}\sum_{j=1}^{j_{\max}}\frac{\omega_{L\nu}}{T_\nu}\left(\frac{1}{\epsilon_{\infty\nu}}-\frac{1}{\epsilon_{0\nu}}\right)\mid F_{if}(q_\nu^j)\mid^2$$
$$\times\int d^2\vec{k}\frac{1}{k^2+(q_\nu^j)^2}\delta(\varepsilon_i-\varepsilon_f\pm\hbar\omega_{L\nu})$$
$$\times(N_{\rm ph}+\tfrac{1}{2}\mp\tfrac{1}{2})\delta_{\vec{k}_i,\vec{k}_f\mp\vec{k}}\,, \qquad (2)$$

where $N_{\rm ph}$ is the phonon occupation number and can be determined by the Planck distribution as

$$N_{\rm ph} = \frac{1}{\exp(\hbar\omega_p/k_BT)-1}\,. \qquad (3)$$

Here $\hbar\omega_p$ is the phonon energy, T is the temperature and k_B is the Boltzmann constant. In equations (1) and (2), the upper sign is for phonon absorption and the lower is for emission, and $F_m(k)$ and $F_{if}(q_\nu^j)$ are the overlap integrals defined as

$$F_m(k) = \left(\frac{1}{\Lambda\Delta^2}\right)^{\frac{1}{2}}\int_L \psi_f^*(z)f_m(k,z)\psi_i(z)dz\,, \qquad (4)$$

where L refers to the length of the entire DBRTS region, and

$$F_{if}(q_\nu^j) = \int_{\text{layer }\nu}\psi_i(z)\sin\left[q_\nu^j(z-z_{0\nu})\right]\psi_f^*(z)dz\,, \qquad (5)$$

where ε_i and ε_f are, respectively, the energies of the initial and final electron states. The states ψ_i and ψ_f are the electron envelope wavefunctions in the initial and final states. For phonon-assisted tunnelling, ψ_i can be calculated according to the transfer-matrix method (Shi *et al.* 1998). Since the width of the final resonant state is very narrow, we can treat the final state as being a completely localised state in the well (Chevoir and Vinter 1989; Turley and Teitsworth 1991*a*, 1991*b*, 1992, 1994; Vassell *et al.* 1983). Equations (1) and (2) are exact and show that scattering rates are functions of the in-plane wave vector $\vec{k}_i$ and energy E_z in the z direction of the initial electron state. Moreover, equations (1), (2), (4) and (5) further clearly indicate that the larger the overlap integral between the initial and final states, the larger the scattering rate. Thus the scattering rate is a sensitive function of E_z. On the contrary, $\vec{k}_i$, in common with $\vec{k}_f$, only occurs in the delta functions in equations (1) or (2) and thus gives an indirect and weak influence on the overlap integral. Since the scattering rate $W(\vec{k}_i, E_z)$ depends strongly on E_z but weakly on $\vec{k}_i$, we can thus assume $W(\vec{k}_i, E_z) \doteq W(0, E_z) \equiv W(E_z)$ for simplicity. For phonon-assisted tunnelling in an asymmetric DBRTS, the simplified scattering rate $W(E_z)$ for phonon emission can be obtained from equations (1) and (2) as follows:

$$W(E_z) = \frac{e^2}{8\varepsilon_0} \sum_{m=1}^{8} \frac{1}{\omega_m(k_p)} |F_m(k_p)|^2 \left(\left| \frac{\hbar^2}{m^*} k_p + \hbar \frac{d\omega_m}{dk} \right|_{k=k_p} \right)^{-1} (N_{\rm ph} + 1)\,, \tag{6}$$

where k_p satisfies

$$\frac{\hbar^2}{2m^*} k_p^2 + \hbar\omega_m(k_p) - (E_z - E_w) = 0\,, \tag{7}$$

for the interface phonon and

$$W(E_z) = \frac{m^* e^2}{\hbar^2 \varepsilon_0} \sum_{\nu=2,3,4} \sum_{j=1}^{j_{\max}} \frac{\omega_{L\nu}}{T_\nu} \left(\frac{1}{\epsilon_{\infty\nu}} - \frac{1}{\epsilon_{0\nu}} \right) \frac{|\, F_{if}(q_\nu^j)\,|^2}{\left((k_p^\nu)^2 + (q_\nu^j)^2 \right)} (N_{\rm ph} + 1)\,, \tag{8}$$

where k_p^ν is given as

$$k_p^\nu = [2m^*(E_z - E_w - \hbar\omega_{L\nu})]^{\frac{1}{2}}/\hbar\,, \tag{9}$$

for the confined bulk-like LO phonon in the left barrier ($\nu = 2$), the well layer ($\nu = 3$) and the right barrier ($\nu = 4$). In equations (7) and (9), $E_z - E_w$ ($= E_{zi} - E_{zf}$) is the energy difference between the incident state and the final resonant state localised in the well. The definitions of q_ν^j, T_ν, Λ, Δ, $f_m(k, z)$ and $z_{0\nu}$, provided in Shi and Pan (1996), are lengthy and not repeated here. Electron–phonon scattering in the emitter and the collector regions has been ignored because the overlap integrals between the emitter (collector) and the final localised resonant state in the well are negligible.

(2b) Phonon-assisted Tunnelling

It is well known that the theoretical values of the coherent tunnelling current density in the valley region of the current-to-voltage curve are much lower than those of experimental observations. This is mainly due to neglecting some complex effects such as: electron–phonon inelastic scattering from the emitter state with a continuous energy spectrum to the quasi-bound state localised in the QW; Γ-X intervalley tunnelling; the effects of band nonparabolicity; impurity and trap state scattering; interface roughness scattering; and the quasi-two-dimensional subband electron tunnelling as pointed out in the Introduction to this paper. In Figs 1 and 2 we show that an electron in the emitter state $\psi(E_z, z)$ can easily escape through the right barrier to the collector. Electron tunnelling in a DBRTS depends sensitively on the bias voltage V. Fig. 1 shows a bias state at resonance ($V = V_{\rm r}$) which corresponds to the peak of the current-to-voltage curve as the electron transmission coefficient $T(E_z)$ through the DBRTS reaches its maximum at that point. For a higher voltage $V > V_{\rm r}$, we have a bias state at the off-resonance condition as shown in Fig. 2, in which the transmission coefficient $T(E_z)$ is small, corresponding to the valley of the current-to-voltage curve. In this case, the energy E_z of an emitter state is higher than the energy E_w of the quasi-bound state (also called resonant state) in the QW. However, phonon-assisted tunnelling may take place if $E_z - E_w \geq \hbar\omega_p$, ω_p being the phonon

frequency. This process leads to an appreciable extra current J_p, where the subscript p stands for the phonon-assisted tunnelling current. Thus, if we neglect other complex effects, we can approximately express the total tunnelling current density as

$$J = J_c + J_p \,, \tag{10}$$

where J_c is the coherent tunnelling current density.

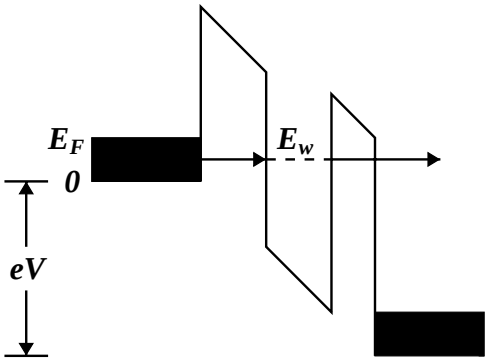

Fig. 1. Electron coherent tunnelling of the resonant bias state ($V = V_\mathrm{r}$), corresponding to the peak of the current-to-voltage curve: E_w represents a quasi-bound state and E_F the Fermi level in the emitter.

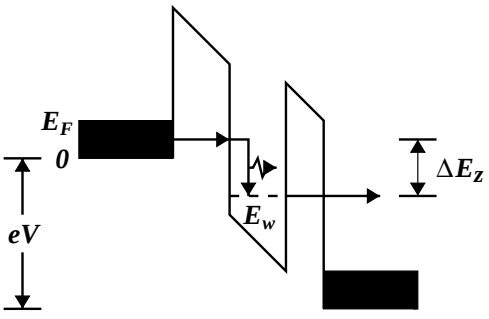

Fig. 2. Phonon-assisted tunnelling of the off-resonant state ($V > V_\mathrm{r}$) corresponding to the valley of the current-to-voltage curve, where ΔE_z denotes the electron-energy loss in the z direction.

In order to construct an expression for J, we make a simple analysis as follows. The J_c term can be written as

$$J_c = en\langle T(E_z)v_z(E_z)\rangle = e\frac{N}{\Omega}\langle T(E_z)v_z(E_z)\rangle\,, \tag{11}$$

where e is the absolute value of the electron charge and N is the total electron number in the electron reservoir with volume Ω. The electron density n is assumed to be constant, and $T(E_z)$ is the electron transmission coefficient, $v_z(E_z)$ the electron moving velocity in the z direction, and $\langle\rangle$ stands for ensemble average. Similarly, we have

$$J_p = \frac{eN\langle W\rangle}{A}\,, \tag{12}$$

where A is the cross-sectional area of the structure and W is the electron–phonon scattering rate, which has been studied in detail in Section 2*a*.

From equation (11) we can obtain the following expression for calculating coherent tunnelling current density, which is known as the Tsu-Esaki (1973) current formula:

$$\begin{aligned} J_c &= J_{c\rightarrow} - J_{c\leftarrow}\,,\\ J_{c\rightarrow} &= \frac{em_{||}k_BT}{2\pi^2\hbar^3}\int_0^\infty T(E_z)\ln\{1+\exp[(E_F-E_z)/k_BT]\}dE_z\,,\\ J_{c\leftarrow} &= \frac{em_{||}k_BT}{2\pi^2\hbar^3}\int_0^\infty T(E_z)\ln\{1+\exp[(E_F-eV-E_z)/k_BT]\}dE_z\,. \end{aligned} \tag{13}$$

Here $J_{c\rightarrow}$ ($J_{c\leftarrow}$) represents the tunnelling current from the emitter (collector) to the collector (emitter). The electron effective mass in the $x-y$ plane which is parallel to the interfaces of the DBRTS is $m_{||}$, and $T(E_z)$ is the electron transmission coefficient through the double barrier structure. The energies E_F and $E_F - eV$ are, respectively, the local Fermi energy levels in the emitter and collector (see Fig. 1 in which the doping concentration in the collector has been assumed to be equal to that in the emitter, and V is the bias voltage). We know from our numerical calculations (cf. Fig. 7) that $J_{c\rightarrow}$ is very important for forming the NDR of DBRTS, which controls the coherent tunnelling current density. Equation (13) clearly shows that the logarithmic function is independent of the structure of the DBRTS; this function can be completely determined from the doping density and the temperature T. On the contrary, the transmission coefficient $T(E_z)$ depends sensitively on the structure of the DBRTS and the bias voltage. Therefore, $T(E_z)$ or, more precisely, the area of the product of $T(E_z)$ with the logarithmic function, is the most important factor for the coherent resonant tunnelling process, and requires detailed analysis.

Let us now derive an explicit expression for the phonon-assisted tunnelling current density J_p. The ensemble average $\langle W\rangle$ of the electron–phonon scattering rate $W(\vec{k}_i, E_z)$ can be expressed as a sum over all of the emitter states as follows:

$$\langle W\rangle = \frac{2}{N}\sum_{\vec{k}_i,E_z} f(\vec{k}_i,E_z)W(\vec{k}_i,E_z)\,. \tag{14}$$

The factor 2 accounts for the electron spin degeneracy, and $f(\vec{k}_i,E_z)$ is the Fermi distribution function. Since the density of states in k-space for the emitter is $\Omega/(2\pi)^3$, with Ω being the volume of the emitter, and $dk_z = dE_z/(\hbar v_z)$, equation (14) can be rewritten as

$$\langle W\rangle = \frac{2}{N}\frac{\Omega}{(2\pi)^2}\int\int dk_i dE_z \frac{k_i}{1+\exp[(E_z+\hbar^2k_i^2/2m_{||}-E_F)/k_BT]}\frac{W(\vec{k}_i,E_z)}{\hbar v_z}\,. \tag{15}$$

Substituting equation (15) into (12), and assuming $W(\vec{k}_i,E_z) \doteq W(0,E_z) \equiv W(E_z)$ as analysed in Section 2*a*, we obtain

$$J_p = \frac{em_{||}k_BTL_e}{2\pi^2\hbar^3}\left(\frac{m_z}{2}\right)^{\frac{1}{2}}\sum_{p=\nu,m}\int_{E_w+\hbar\omega_p}^{\infty}\frac{\ln[1+e^{(E_F-E_z)/k_BT}]}{\sqrt{E_z}}W_p(E_z)dE_z\,, \tag{16}$$

with L_e the emitter length, m_z the electron effective mass for the motion along the z-direction in the emitter, $\nu = 2,3,4$ the index for confined bulk-like LO phonon modes in the left-barrier, the well and the right-barrier layers, and $m = 1,2,3,4,5,6,7,8$ the index for the eight interface phonon modes. The electron–phonon scattering rate in the ν^{th} layer is $W_\nu(E_z)$, and $W_m(E_z)$ is the electron–m^{th}-interface phonon modes scattering rate.

It is worth mentioning that equation (16) represents only the phonon-assisted tunnelling current from the emitter-to-collector tunnelling via a phonon emission. More accurately, it should be subtracted by the back current from collector-to-emitter tunnelling by means of a phonon absorption. From Shi *et al.* (1998) and Fig. 2, we know that the electron–phonon scattering rate for collector-to-emitter tunnelling is much smaller than that for the emitter-to-collector tunnelling. There are two reasons for the disparity in backward versus forward scattering rates. One reason is that the overlap integral of the electron envelope wave functions between the initial state (plane waves incident from the collector) and the final one (localised states in the emitter) for the collector-to-emitter tunnelling is much smaller than that for the emitter-to-collector tunnelling process with the final state localised in the QW. The other reason is that the phonon occupation number $N_{\text{ph}}+1$ for phonon emission is larger than N_{ph} for absorption according to equation (3). Hence the phonon-assisted tunnelling current from collector-to-emitter tunnelling via a phonon absorption is much smaller than that from emitter-to-collector tunnelling by virtue of a phonon emission and has been ignored in equation (16) due to the smaller scattering rate $W_{\text{p}}(E_{\text{z}})$ for collector-to-emitter tunnelling. This has also been confirmed by Turley and Teitsworth (1991*a*, 1991*b*, 1992, 1994).

Comparing equations (13) and (16), we can see that they are similar in appearance. The factor of the logarithmic function is the same in both. The only difference is that the electron transmission coefficient $T(E_z)$ in $J_{c\rightarrow}$ is replaced by $W_p(E_z)\sqrt{m_z/2E_z}L_e$ in the expression for J_p. Moreover, similar to $T(E_z)$, $W_p(E_z)$ depends on the structure of DBRTS and the bias voltage. Although

equation (16) is similar to (13) in appearance, the numerical calculation of J_p is much more difficult than that of the coherent tunnelling current J_c. In the following section, we present numerical examples for the scattering rates and tunnelling currents. Our numerical calculation (see Fig. 8 below) shows that J_p mainly comes from the electron higher frequency interface phonons (especially the interface phonons localised at either interface of the left barrier) scattering, which is very important for understanding the phonon-assisted tunnelling process.

3. Numerical Results and Discussion

As an application of the theory given in Section 2, we have performed numerical calculations for the electron–phonon scattering rate and for the coherent tunnelling current and the phonon-assisted tunnelling current in a specially designed asymmetric DBRTS $\mathcal{A}(0\cdot25,\ 20\ \text{Å})$, where we define

$$\mathcal{A}(x,d) \equiv \text{GaAs}(1000\ \text{Å})/\text{Al}_x\text{Ga}_{1-x}\text{As}(30\ \text{Å})/$$
$$\text{GaAs}\ (60\ \text{Å})/\text{Al}_{0\cdot3}\text{Ga}_{0\cdot7}\text{As}(d)/\text{GaAs}(1000\ \text{Å}).$$

The physical parameters used in our calculations are the same as those of Shi *et al.* (1997). Moreover, we assume $m_{||} = m_z$. The doping concentration in the emitter and the collector is the same and is fixed at 10^{18} cm^{-3}.

Fig. 3 depicts the dispersion of the interface modes for structure $\mathcal{A}(0\cdot25,$ 20 Å). Eight interface modes with different energies are found, which are very important for further investigating electron–phonon scattering and phonon-assisted tunnelling in the DBRTS. We can see from Fig. 3 that the four lower-frequency modes occupy a much narrower frequency band than the four higher-frequency modes. The dispersion of the interface modes is obvious in the case of the wavenumber $k \leq 0\cdot1$ Å^{-1} and can be ignored in the region of $k > 0\cdot1$ Å^{-1}.

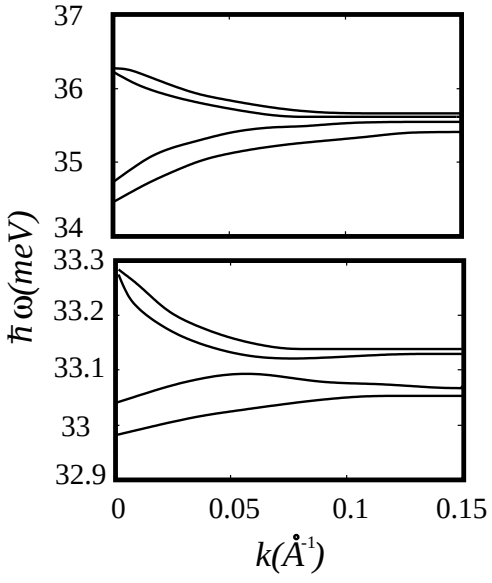

Fig. 3. Dispersion curves of the interface modes for structure $\mathcal{A}(0\cdot25,\ 20$ Å).

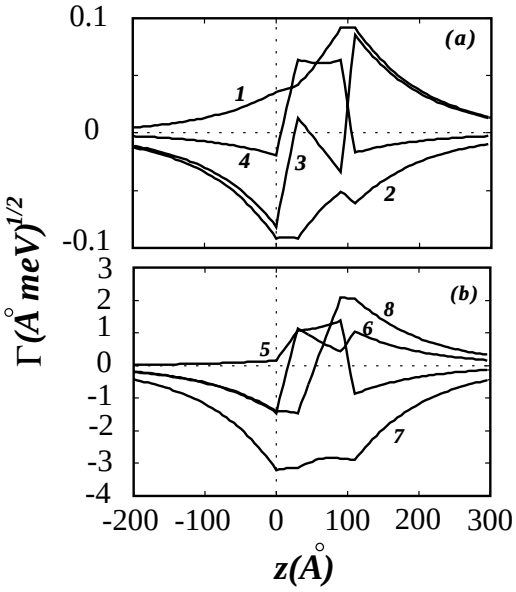

Fig. 4. Spatial dependence of the coupling functions $\Gamma(k,z)$ divided by $(\hbar e^2/A\varepsilon_0)^{\frac{1}{2}}$ for the interaction between an electron and interface optical phonons for structure $\mathcal{A}(0{\cdot}25,\ 20$ Å) ($k = 0{\cdot}01$ Å^{-1}). Here the numbers by the curves represent the interface-phonon frequency in order of increasing magnitude: (*a*) for the four lower-frequency modes and (*b*) for the four higher-frequency modes. The interfaces are localised at $z = 0$, 30, 90 and 110 Å respectively.

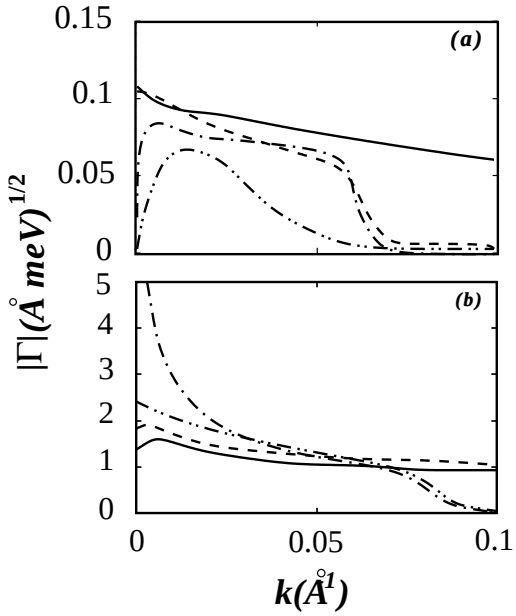

Fig. 5. Absolute values $|\Gamma(k,z)|$ divided by $(\hbar e^2/A\varepsilon_0)^{\frac{1}{2}}$ as functions of k for the same structure as in Fig. 3: (*a*) for the four lower-frequency modes and (*b*) for the four higher-frequency modes. Here solid lines represent the interaction of an electron with the modes 1 and 5 [e–p(1) and e–p(5)], dashed lines represent e–p(2) and e–p(6), dash–dot lines represent e–p(3) and e–p(7), and dash–dot–dot lines represent e–p(4) and e–p(8), respectively.

We know from previous studies (Shi and Pan 1995, 1996; Shi *et al.* 1997) that the electron–interface–phonon coupling function $\Gamma(k, z)$ in semiconductor heterostructures is a very complicated function of coordinate z and wavenumber k. We further investigate the characteristic of $\Gamma(k, z)$ in Figs 4 and 5 so that the electron–phonon interaction can be understood very well. Fig. 4 shows the $\Gamma(k, z) - z$ relation for the same DBRTS as in Fig. 3, where (a) is for the four lower-frequency modes 1, 2, 3 and 4, and (b) is for the four higher-frequency modes 5, 6, 7 and 8 named in order of increasing frequency. The electron–phonon attractive or repulsive interactions are produced due to the complicated polarisation of the crystal. The plots shown in Fig. 4 reveal an electron interaction with different mode peaks at different interfaces. For example, the electron interaction with mode 7 [denoted as e–p(7)] peaks at the $z = 0$ and 30 Å interfaces (i.e. either interface of the left barrier), which is very important for understanding the phonon-assisted tunnelling process (cf. Fig. 8). Fig. 5 presents the absolute values $|\Gamma(k, z)|$ as a function of wavenumber k for four lower-frequency modes in (a) and for four higher-frequency modes in (b). We can see from Fig. 5 that the electron–phonon coupling function $\Gamma(k, z)$ is a very complicated function of k. For example, the e–p(7) interaction decreases rapidly for $0 < k \leq 0{\cdot}01$ Å^{-1} and slowly for $0{\cdot}01$ Å$^{-1} < k < 0{\cdot}08$ Å^{-1}, and then decreases rapidly again for $k > 0{\cdot}08$ Å^{-1}. Fig. 5 indicates that the seventh interface mode is much more important than the other modes in our asymmetric DBRTS. The results shown in Fig. 8a also strongly support this conclusion. Figs 4 and 5 clearly show that the four higher-frequency modes produce intensive polarisation in the DBRTS and cause a large interaction with electrons. On the contrary, the four lower-frequency modes give a weak interaction with electrons compared with the higher-frequency modes, which can be ignored. In the following calculations, we will thus only consider the contribution of the four higher-frequency modes to the scattering rate and the phonon-assisted tunnelling current for simplicity.

Fig. 6 shows the scattering rate divided by $(N_{\rm ph}+1)$ as a function of the incident electron energy E_z for the same structure as in Fig. 3 at the bias voltage $V = 150$ mV. The doping concentration in the emitter (and in the collector) is assumed to be $n = 10^{18}$ cm^{-3}, and the corresponding Fermi energy level at room temperature is $E_F = 42{\cdot}5$ meV. Fig. 6 shows that the contribution of interface phonons is larger than that of LO bulk-like phonons for lower incident electron energies ($E_z \leq 180$ meV). We know from the Fermi distribution function that the emitter states are appreciably populated only for $E_z \leq E_F + k_B T = 68{\cdot}3$ meV (as $T = 300$ K). Hence, we can infer that the interface phonons are much more important than the confined bulk-like LO phonons for the phonon-assisted tunnelling current. Our following numerical calculations (cf. Fig. 8c) strongly support this analysis. Fig. 6 also indicates that the total scattering rate has its maximum at $E_z \doteq 154$ meV. We know from our numerical calculations that $E_z = 154$ meV corresponds to the second resonant level at $v = 150$ mV. The overlap integral between the confined state in the well and the second resonant state has the largest value. Hence, the electron–phonon scattering rate has a maximum at $E_z \doteq 154$ meV. In order to further investigate the influence of the conduction band nonparabolicity on electron–phonon scattering, we have calculated the electron–phonon scattering rate in considering the subband nonparabolicity. The result is presented as the dash–dot–dot line in the figure which shows that the subband nonparabolicity

has a large influence on the electron–phonon scattering. The position of the peak shifts to a lower energy, and its value decreases under the influence of the subband nonparabolicity. Moreover, it is interesting to compare the relaxation time $1/W_p(E_z)$ with the electron dwell time in the quantum well. Fig. 6 shows that the relaxation time in our DBRTS is of the order of 10 to 100 ps. The dwell time in a symmetric $Al_{0\cdot4}Ga_{0\cdot6}As/GaAs/Al_{0\cdot4}Ga_{0\cdot6}As$ with a well width of 50 Å is also of the order of 10 to 100 ps (Liu and Sollner 1994). Although an exact result for the dwell time is expected for our asymmetric structure, the electron dwell time and the relaxation time are comparable.

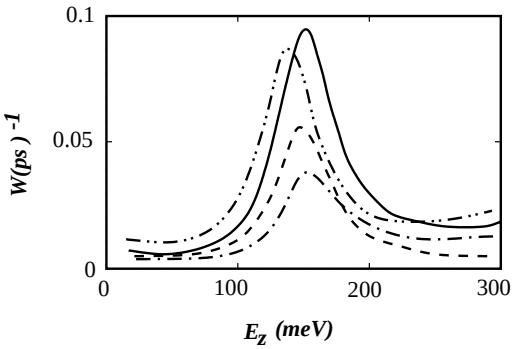

Fig. 6. Electron–phonon scattering rate W divided by $(N_{\rm ph}+1)$ as a function of the incident electron energy E_z for the structure in Fig. 3 at the bias voltage $V = 150$ mV. The dashed line and dash–dot line represent, respectively, the contribution of the interface phonons and confined bulk-like LO phonons, and the solid line is their sum in the absence of subband nonparabolicity. The dash–dot–dot line is the total scattering rate including subband nonparabolicity.

Fig. 7 shows the coherent tunnelling current-to-voltage curve calculated at room temperature for the same DBRTS as in Fig. 3, in which the subband nonparabolicity is included. This figure clearly indicates that the NDR of the DBRTS is formed when the electrons tunnel from the emitter to the collector ($J_{c\rightarrow}$). The tunnelling current from the collector to the emitter ($J_{c\leftarrow}$) monotonically decreases when the applied bias voltage increases, and this current can be ignored when the voltage is large enough, e.g. $V > 150$ mV. Therefore, in the following we are only concerned with the characteristics of $J_{c\rightarrow}$ and its dependence on the structure parameters of the DBRTS.

In the case where subband nonparabolicity is included, phonon-assisted tunnelling current-to-voltage curves are shown in Fig. 8 at room temperature for the structure $\mathcal{A}(0\cdot25,\ 20$ Å). Fig. 8*a* shows the tunnelling current assisted by the four higher-frequency interface phonon modes and their sum. We can see from Fig. 8*a* that the seventh interface mode, which is localised at either interface of the left barrier, is the most important of all of the interface modes, and this result is consistent with the results shown in Figs 4 and 5. The total interface phonon-assisted tunnelling current is very complicated and has two peaks as the voltage increases. Fig. 8*b* gives the confined bulk-like LO phonon-assisted tunnelling current density in the structure $\mathcal{A}(0\cdot25,\ 20$ Å). This figure clearly indicates that the phonon-assisted tunnelling current from the LO phonons in the

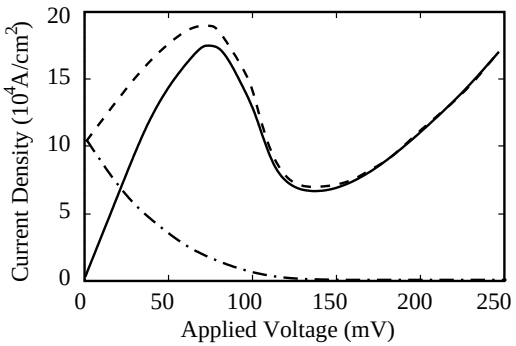

Fig. 7. Coherent tunnelling current-to-voltage curve calculated at room temperature for the same DBRTS as in Fig. 3. The dashed line is for electron tunnelling from the emitter to the collector, the dash–dot line is for electron tunnelling from the collector to the emitter and the solid line is the total coherent tunnelling current density.

well is much larger than those from the LO phonons in the two barrier layers and has a complicated behaviour when the bias voltage increases. Fig. 8*c* presents the total phonon-assisted tunnelling current density including the interface and the confined bulk-like LO phonons. We can see from Fig. 8*c* that the interface phonon-assisted tunnelling current is larger by one order of magnitude than the confined LO-phonon-assisted tunnelling current for our chosen sample. This is because the interface-phonon scattering is much more important than the confined LO phonon scattering (cf. Fig. 6). Fig. 8*c* also shows that the total phonon-assisted tunnelling current is a very complicated function of the applied voltage and has two peaks. This is similar to the result of Mori *et al.* (1992). Moreover, Fig. 8 clearly indicates that the phonon-assisted tunnelling current is mainly determined by scattering between electrons and higher frequency interface phonons (especially the interface phonons localised at either interface of the left barrier). This physical picture of the phonon-assisted tunnelling is important for further understanding the phonon-assisted tunnelling process and for designing better resonant tunnelling devices.

Fig. 9 shows the total current-to-voltage curve at room temperature for the same DBRTS as in Fig. 3, including coherent and phonon-assisted tunnelling currents. This figure shows that phonon-assisted tunnelling increases the valley current and decreases the PVR. The results shown in Fig. 9 are similar to those of Roblin and Liou (1993) and Mains and Haddad (1988), in which very different methods were adopted.

Fig. 10 represents the current-to-voltage characteristic curves at different temperatures and the influence of the conduction band nonparabolicity on the current-to-voltage curve for the structure $\mathcal{A}(0{\cdot}25,\ 20\ \text{Å})$. This figure shows that at low temperature $T = 100$ K, the current-to-voltage curve has a larger peak, a lower valley, and a larger PVR ($=6{\cdot}17$). As for the result of $T = 300$ K (room temperature), we find that the current-to-voltage curve has a slightly lower peak, a larger valley current, and a small PVR ($=2{\cdot}47$). Moreover, Fig. 10 also shows that the width of the NDR region at room temperature is narrower than that at low temperature. We can also see from Fig. 10 that the subband nonparabolicity

has a large influence on the current-to-voltage characteristic curve. For example, if we consider the subband nonparabolicity, the PVR of the current-to-voltage curve will be reduced from 2·74 (without the nonparabolicity effect) to 2·47. Hence, the subband nonparabolicity is also an important factor which must be considered in resonant tunnelling processes.

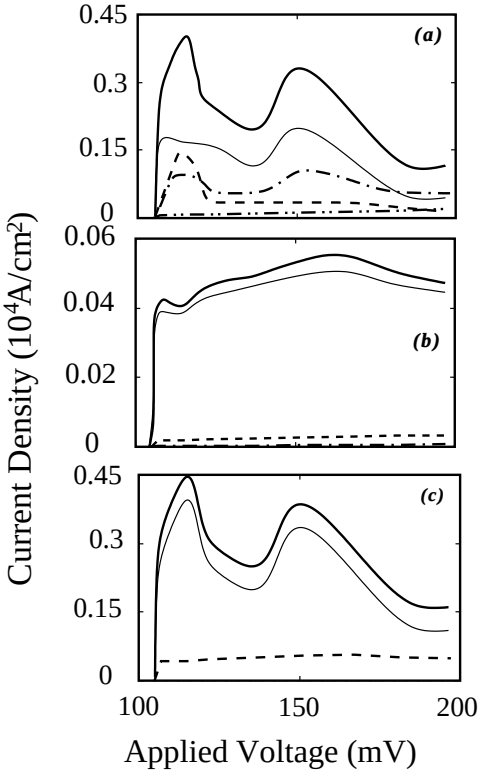

Fig. 8. Phonon-assisted tunnelling current-to-voltage curves at room temperature for structure $\mathcal{A}(0\cdot25, 20$ Å), including the subband nonparabolicity: (*a*) Interface phonon-assisted tunnelling: the dashed line represents the fifth interface modes contribution for the tunnelling current, the dash–dot–dot line for the sixth mode, the thin solid line for the seventh mode, the dash–dot line for the eighth mode and the heavy solid line is their sum. (*b*) LO phonon-assisted tunnelling: the dashed line represents the confined LO phonon in the left barrier ($Al_{0\cdot25}Ga_{0\cdot75}As$) contribution for the tunnelling current, the dash–dot line for the LO phonon in the right barrier ($Al_{0\cdot3}Ga_{0\cdot7}As$), the thin solid line for the confined bulk-like LO phonon in the well (GaAs) and the heavy solid line is their sum. (*c*) Interface phonon-assisted tunnelling current (thin solid line), confined LO phonon-assisted tunnelling current (dashed line) and their sum (heavy solid line).

In order to compare the current-to-voltage characteristics in asymmetric and symmetric DBRTSs and to explore the advantages of the asymmetric DBRTS, we have also studied the tunnelling current density for DBRTS $\mathcal{A}(0\cdot3, d)$ with $d = 20$, 30 and 40 Å. The calculated results show that when the right barrier thickness d increases, the peak current decreases, the PVR increases, and the peak position shifts towards higher bias voltage. These three characteristics are in agreement with recent experimental results (Schmidt *et al.* 1996). Moreover, we have also

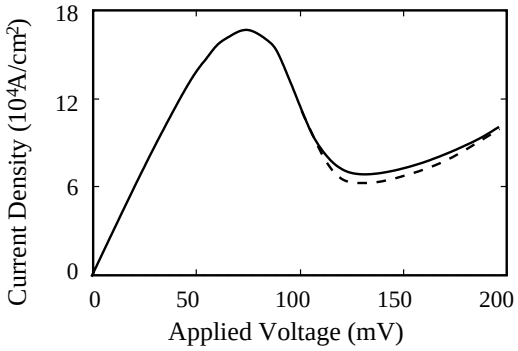

Fig. 9. Total current-to-voltage characteristic curve at room temperature considering the subband nonparabolicity for the same asymmetric DBRTS as in Fig. 3. The dashed line stands for the coherent tunnelling current density. The solid line is the total tunnelling current density combining coherent and phonon-assisted tunnelling currents.

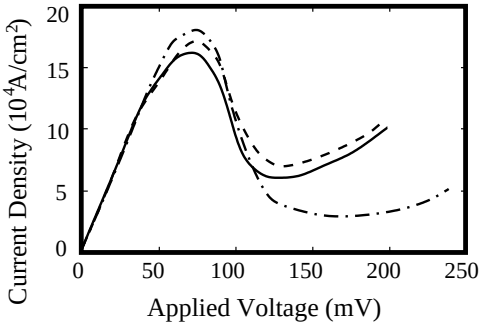

Fig. 10. Current-to-voltage characteristic curves including coherent and phonon-assisted tunnelling for the same asymmetric DBRTS as in Fig. 3 at $T = 100$ K (the dash–dot line includes the subband nonparabolicity) and $T = 300$ K (the solid line ignores the nonparabolicity, and the dashed line includes the nonparabolicity).

studied the current-to-voltage characteristics for $\mathcal{A}(x,\ 30\ \text{Å})$ with $x = 0{\cdot}2$, $0{\cdot}25$, $0{\cdot}3$ and $0{\cdot}35$. The calculated results are shown in Fig. 11. This figure clearly indicates that the peak current and absolute value of the negative differential conductivity are higher for a structure with lower x and hence lower left barrier. We can attribute the above trend to two physical reasons. First, a structure with a lower left barrier has a higher peak transmission coefficient. Secondly, the bias raises the left barrier top to the right one. A structure with a lower left barrier can compensate the latter effect and hence can cause the left and right barrier tops to locate at similar energy levels under resonant bias. For example, the left and right barrier tops in the $x = 0{\cdot}2$ asymmetric DBRTS under resonance bias are closer than that in the symmetric one with $x = 0{\cdot}3$. As is known, a DBRTS with the same or similar left and right barrier potential can achieve an enhanced transmission coefficient. Based on the above two physical reasons, we can understand why an asymmetric DBRTS with lower left barrier height can improve performance. These theoretical results need to be confirmed by experiment.

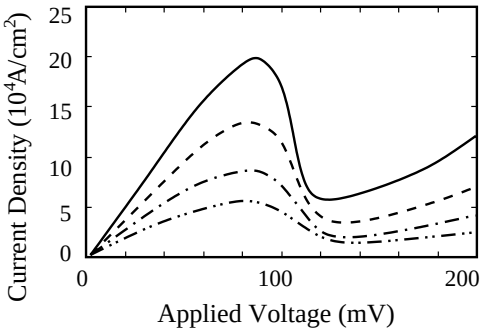

Fig. 11. Current-to-voltage curves calculated at room temperature for structures $\mathcal{A}(x,\ 30\ \text{Å})$ with doping density $n = 10^{18}\ \text{cm}^{-3}$. The solid line is for $x = 0{\cdot}2$, the dashed line for $x = 0{\cdot}25$, the dash–dot line for $x = 0{\cdot}3$ (symmetric DBRTS), and the dash–dot–dot line for $x = 0{\cdot}35$.

4. Summary

In this paper, an important physical picture on coherent and phonon-assisted tunnelling in a general asymmetric DBRTS is presented. The electron–phonon interaction, scattering and the phonon-assisted tunnelling current were investigated in detail for a specially designed asymmetric structure $\mathcal{A}(0{\cdot}25,\ 20\ \text{Å})$, within the framework of the dielectric continuum model. All of the phonon modes were included and the conduction band nonparabolicity was also considered. The importance of the different phonon modes was analysed. The current-to-voltage characteristic curves were analysed and compared between asymmetric and symmetric DBRTS. The main results obtained in the present paper can be summarised as follows:

(1) The most important characteristics of the coherent tunnelling current-to-voltage curve can be directly determined by both the width of the resonant level and the peak value of the transmission coefficient on the resonant level. The NDR of a DBRTS is formed and determined by electron tunnelling from the emitter to the collector.

(2) There are eight interface phonon modes in a DBRTS. Different modes are localised at different heterointerfaces. The four higher-frequency modes (i.e. modes 5 to 8, especially the seventh one which peaks at either interface of the left barrier) are much more important than the four lower-frequency modes (i.e. modes 1 to 4) for the electron–phonon interaction, electron–phonon scattering, and phonon-assisted tunnelling. The confined LO phonons in the well layer are more important than those in the two barrier layers. The interface phonons are much more important than the confined LO phonons.

(3) The peak current is reduced, the position of peak current is shifted to a higher voltage, and the PVR is enlarged if the right-barrier width is increased when the two barriers have the same height. The peak current is increased by suitably decreasing the left-barrier height when the two barriers have the same width.

(4) The PVR of a RTD at a lower temperature is larger than that at a higher temperature. Moreover, the higher the temperature, the narrower the width of the NDR region of the tunnelling current-to-voltage curve.

(5) The phonon-assisted tunnelling current mainly comes from the scattering of electron higher frequency interface phonons (especially the interface phonons localised at either interface of the left barrier), which increases the valley current and decreases the PVR of the DBRTS.

(6) The subband nonparabolicity has a significant influence on electron–phonon scattering, phonon-assisted tunnelling, and the current-to-voltage characteristic of a RTD.

As stated above, phonon-assisted tunnelling and subband nonparabolicity are two important factors for increasing the valley current of the DBRTS. An asymmetric DBRTS with a suitably designed structure may have an improved performance over the commonly used symmetric DBRTS. The results obtained in this paper are useful for analysing and understanding scattering process and decoherence and for potentially important resonant tunnelling device designs and applications in the near future.

References

Cai, W., Zheng, T. F., Hu, P., Yudanin, B., and Lax, M. (1989). *Phys. Rev. Lett.* **63**, 418.
Chang, L. L., Esaki, L., and Tsu, R. (1974). *Appl. Phys. Lett.* **24**, 593.
Chen, J., Chen, J. G., Yang, C. H., and Wilson, R. A. (1991). *J. Appl. Phys.* **70**, 3131.
Chevoir, F., and Vinter, B. (1989). *Appl. Phys. Lett.* **55**, 1859.
Goldman, V. J., Tsui, D. C., and Cunningham, J. E. (1987). *Phys. Rev.* B **36**, 7635.
Leadbeater, M. L., Alves, E. S., Eaves, L., Henini, M., Hughes, O. H., Celeste, A., Portal, J. C., Hill, G., and Pate, M. A. (1989). *Phys. Rev.* B **39**, 3438.
Liu, H. C., and Sollner, T. C. L. G. (1994). *In* 'High Speed Heterostructure Devices Semiconductors and Semimetals' (Eds R. A. Kiehl and T. C. L. G. Sollner), Vol. 41, p. 359 (Academic: Boston).
Mains, R. K., and Haddad, G. I. (1988). *J. Appl. Phys.* **64**, 5041.
Mizuta, H., and Tanoue, T. (1995). 'The Physics and Applications of Resonant Tunnelling Diodes' (Cambridge University Press).
Mori, N., Taniguchi, K., and Hamaguchi, C. (1992). *Semicond. Sci. Technol.* **7**, B83.
Orellana, P., Claro, F., Anda, E., and Makler, S. (1996). *Phys. Rev.* B **53**, 12967.
Roblin, P., and Liou, Wan-Rone. (1993). *Phys. Rev.* B **47**, 2146.
Schmidt, T., Tewordt, M., Haug, R. J., Klitzing, K. v., Schönherr, B., Grambow, P., Förster, A., and Lüth, H. (1996). *Appl. Phys. Lett.* **68**, 838.
Shi, J-J., and Pan, S.-H. (1995). *Phys. Rev.* B **51**, 17681.
Shi, J-J., and Pan, S.-H. (1996). *J. Appl. Phys.* **80**, 3863.
Shi, J.-J., Sanders, B. C., and Pan, S.-H. (1998). *Euro. Phys. J.* B **4**, 113.
Shi, J.-J., Zhu, X.-Q., Liu, Z.-X., Pan, S.-H., and Li, X.-Y. (1997). *Phys. Rev.* B **55**, 4670.
Sun, J. P., Haddad, G. I., Mazumder, P., and Schulman, J. N. (1998). *Proc. IEEE* **86**, 641.
Tsu, R., and Esaki, L. (1973). *Appl. Phys. Lett.* **22**, 562.
Turley, P. J., and Teitsworth, S. W. (1991*a*). *Phys. Rev.* B **44**, 3199.
Turley, P. J., and Teitsworth, S. W. (1991*b*). *Phys. Rev.* B **44**, 8181.
Turley, P. J., and Teitsworth, S. W. (1992). *J. Appl. Phys.* **72**, 2356.
Turley, P. J., and Teitsworth, S. W. (1994). *Phys. Rev.* B **50**, 8423.
Vassell, M. O., Lee, J., and Lockwood, H. F. (1983). *J. Appl. Phys.* **54**, 5206.
Wingreen, N. S., Jacobsen, K. W., and Wilkins, J. W. (1989). *Phys. Rev.* B **40**, 11834.

Manuscript received 6 April, accepted 21 May 1999